FACULTY OF SCIENCE
UNIVERSITY OF COPENHAGEN

Experiments with ultra precise light sources

Amalie Christensen and Stefan Alaric Petersen

May 27, 2011

Supervisors: Jan Westenkær Thomsen
Philip G. Westergaard

Preface

This project has been carried out during the winter and spring of 2011 as a part of the bachelor program at the Niels Bohr Institute at the University of Copenhagen. The thesis is intended to be comprehensible for students at our own level.

We would like to thank our supervisors Jan W. Thomsen and Philip G. Westergaard who have been of tremendous support throughout the entire project. They have always been willing to help, and provided a most pleasant working environment.

Stefan Alaric Petersen
December 24, 1988

Amalie Christensen
August 28, 1988

Abstract

Taking advantage of atomic transition frequencies, atomic clocks provide an unmatched time reference with accuracies better than 10^{-17}. These high accuracy clocks are essential in modern research and technology. By locking a laser to a certain atomic transition, the laser frequency can be very accurately stabilized, essentially constructing a clock. In order to properly lock this clock laser frequency to the atomic transition, great precision of the clock laser frequency is demanded.

In the construction of a ^{25}Mg clock in the Ultra Cold Atoms group of the Niels Bohr Institute at the University of Copenhagen, the clock laser is stabilized using multiple Pound-Drever-Hall schemes. This thesis will be concerned with one of these Pound-Drever-Hall schemes. We are concerned with having a large laser capture range, providing a lock that removes mainly low frequency noise.

The properties of the Pound-Drever-Hall scheme are investigated, and the noise of the laser characterized. We find that our lock provides a factor of 10 improvement on the laser linewidth, readying the laser for further noise-reduction. We examine the laser power spectral density and identify possible sources of noise.

Resumé

Med en precision bedre end 10^{-17} giver atom-ure en enestående god tidsreference ved at udnytte atomare transitionsfrekvenser. Disse højpræcisionsure er essentielle i såvel moderne videnskab som teknologi. Ved at fastlåse en laser til en specifik atomar overgang, kan laserfrekvensen stabiliseres med stor nøjagtighed. Med andre ord kan man konstruere et ur. For at låse frekvensen af clock-laseren til den atomare overgang er det nødvendigt med stor nøjagtighed af clock-laser frekvensen.

I konstruktionen af et ^{25}Mg ur i Ultra Cold Atoms gruppen på Niels Bohr Institutet ved Københavns Universitet, er clock-laseren stabiliseret ved hjælp af flere Pound-Drever-Hall systemer. Dette projekt omhandler konstruktionen af et af disse Pound-Drever-Hall systemer. Vi ønsker at have et stort frekvensinterval indenfor hvilket, det er muligt at låse laseren, og vi opnår derfor en lås, der hovedsageligt fjerner lavfrekvent støj.

Egenskaberne ved Pound-Drever-Hall systemet undersøges, og støjen karakteriseres. Vi finder at vores lås resulterer i en forbedring af clock-laserens liniebredde med en faktor 10, og derved forbereder laseren til en yderligere støjreduktion. Vi undersøger desuden clock-laserens effektmæssige spektral densitet (power spectral density) for at identificere mulige støjkilder

List of Figures

Contents

1 Introduction

Precise clocks are essential for fundamental science. With a well known frequency standard, one is able to conduct measurements on other physical quantities with very high precision. Length, for instance, can be measured to a high degree of accuracy by measuring the time it takes an electromagnetic pulse to travel the distance of interest. This is possible because the speed of light, c, is *defined* to be exactly 299 792 458 m/s. Other units that can be measured using a frequency standard include weight, using a watt-balance [1], and even voltage through the Josephson effect [2]. It is not only fundamental science that is dependent on precise time measurement, but also everyday life technology such as the Global Positioning System (GPS) depends critically on precise time measurement.

To build a clock you need an oscillator and a method of counting oscillations. This has been done by various means through history - from simple mechanical pendulums to atomic clocks. In the middle of the 20th century the first Cs clock was developed, with an accuracy of $\sim 10^{-10}$, and since 1967 the second has been defined as exactly 9 192 631 770 periods of the light originating from the transition between the two hyperfine levels of the ground state ^{133}Cs atom [3].

Scientific research has continued to increase the accuracy of atomic clocks, and today many different types of clocks exist, exploiting the properties of a wide range of atoms. Atomic clocks provide some of the most precise measurements in physics, with accuracies better than 10^{-17} [4].

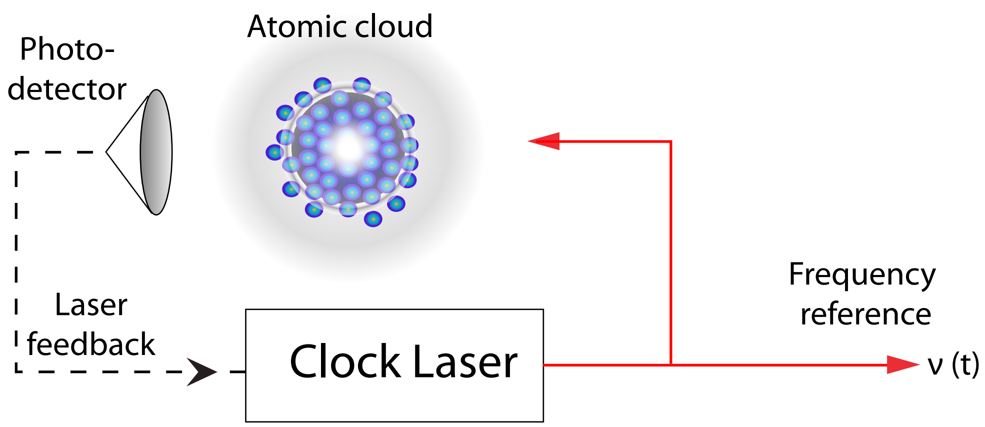

Figure 1: *Red lines indicate laser light, whereas the dashed line indicates an electrical feedback signal. The laser shines light onto a sample of atoms. The detector collects the atoms' response to the laser light and a feedback signal is supplied to the laser adjusting the frequency to resonance. The locked laser provides the frequency reference.*

The concept of an atomic clock is displayed in figure 1. The laser shines light onto a sample of atoms. The atoms' response to the laser light is collected by the photo-detector, and a feedback signal is supplied to the laser. If the laser is slightly out of resonance with the atomic transition, the laser is adjusted by the feedback signal. When locked properly to the atomic transition, the laser frequency will provide a frequency reference corresponding to the given atomic transition.

In the laser laboratory at the Niels Bohr Institute (NBI) of the University of Copenhagen, the forbidden singlet $^1S_0 \leftrightarrow ^3P_0$ triplet transition of ^{25}Mg is investigated as a candidate for an atomic clock transition. The laser used for probing the ^{25}Mg atoms needs to have a very small linewidth as this will yield a better stability of the system.

Narrowing the laser linewidth is the goal of this thesis, and it will be done by applying a Pound-Drever-Hall (PDH) stabilization scheme to the laser. This thesis is organized as follows:

Section 2 gives an overview of the relevant theory. The theoretical considerations of the PDH scheme are presented followed by the essentials of noise analysis.

Section 3 reviews the essentials of the experimental PDH setup, we have built, and outlines our considerations regarding the setup.

Section 4 presents the experimental results for the efficiency of the PDH stabilization. The PDH setup and the noise spectrum of the laser are characterized.

Section 5 discusses the results and offers an outlook for future improvements to the setup.

Section 6 concludes the thesis.

2 Theoretical considerations

In this section, we present an overview of the theory behind our project. We introduce a technique known as the Pound-Drever-Hall scheme that enables us to stabilize the frequency of our laser to an optical resonator [5]. Some of the advantages of this technique are discussed, and an explanation of the considerations behind the method is given. Subsequently, we outline the essentials of noise analysis, explaining the main noise characteristics and give a method of obtaining a value of the laser linewidth.

2.1 Pound-Drever-Hall error-signals

The Pound-Drever-Hall locking scheme is employed to minimize the frequency fluctuations of our laser, and will allow us to reduce the linewidth of the laser dramatically.

The total setup contains two PDH-systems. The PDH-system we have built is based on a low-finesse (~ 100) cavity and will serve as a pre-stabilization in order to successfully use the second PDH-system containing a very high-finesse ($\sim 86\,000$) cavity [6]. The finesse is a measure of the reflectivity of the mirrors and proportional to the photon lifetime in the cavity. This second high-finesse PDH-system is too sensitive to operate with large noise fluctuations making the pre-stabilization necessary.

2.1.1 Motivation for the PDH technique

The essence of the PDH technique is to lock a laser to an optical resonator. This is done by generating a signal, referred to as the error-signal, containing information about the detuning of the laser from the cavity resonance.

The PDH setup is conceptually displayed in figure 2 and consists of the main elements: a Fabry-Perot cavity (FP), a polarizing beam splitter (BS), a $\lambda/4$–plate, an electro-optic modulator (EOM) and the electronics, displayed in a blue box in figure 2. The electronics manipulate the reflected light from the Fabry-Perto cavity, and produce the error-signal providing feedback to the laser.

If we monitor a fraction of the laser beam with a photo diode after passing it through a Fabry-Perot cavity, we will see a Lorentzian intensity profile in the frequency domain (this part of the beam is *not shown* on figure 2). In the Fabry-Perot cavity, we make sure only one mode resonates, and we will subsequently refer to this as the cavity-signal. Any deviation of the laser frequency from cavity resonance will lower the intensity of the cavity-signal. This cavity-signal will be symmetric with respect to the resonance frequency and does not allow us to distinguish between a positive or negative detuning from resonance.

The PDH technique solves this problem by monitoring the *reflected signal* from the cavity. The reflected signal will be a mixture of the immediately reflected signal and the leaking cavity-field, providing a sensitive phase-dependency close to resonance. In the following we will show how the error-signal can be obtained from the reflected signal, and how we use it to correct the laser frequency.

The error-signal of the PDH-scheme also has the advantage of only being sensitive to power fluctuations caused by frequency fluctuations - not to power fluctuations of the laser itself.

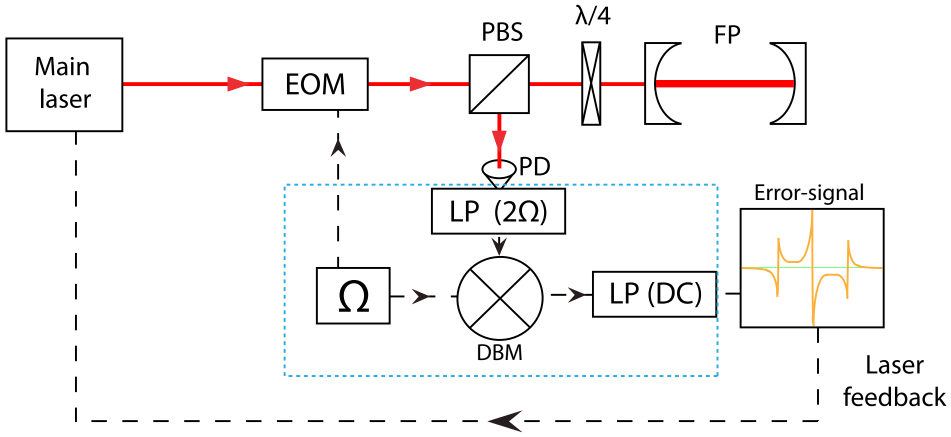

Figure 2: *A simplified view of the PDH setup. Red lines indicate laser light and dashed lines indicate electrical signals. The phasemodulated light from the EOM resonates in the Fabry-Perot cavity (FP). A mix of leaking and reflected signals from the cavity is directed towards a photodiode (PD) by use of a polarising beam splitter (PBS), and manipulated to produce our feedback signal. The electrical components shown here are a frequency generator* Ω*, two low-pass filters (LP) and a mixer (DBM).*

2.1.2 Obtaining the error-signal

The reflected cavity-signal

We consider a symmetric cavity of length L with no losses and mirror amplitude reflection coefficient r. We write the incident wave as $E_{in} = E_0 e^{i\omega t - \mathbf{k}\cdot\mathbf{x}}$, where the phase factor is choosen to be equal to unity at the surface of the cavity entrance-mirror.

The reflected beam E_{re} off the Fabry-Perot cavity, is the sum of the immediately reflected field from the mirror surface rE_{in} and the leaking cavity field, which consists of field components having completed a different number of roundtrips in the cavity:

$$E_{re} = rE_{in} - \underbrace{E_{in}\left(t^2 r \cdot e^{-i\omega\frac{2L}{c}} + t^2 r^3 \cdot e^{-i\omega 2\frac{2L}{c}} + t^2 r^5 \cdot e^{-i\omega 3\frac{2L}{c}} + ...\right)}_{\text{Leaking cavity field}}. \tag{2.1}$$

Whereas the frequency of the reflected and leaking fields in eq.(2.1) will always be the same, their phase-difference will depend strongly on the value of the frequency and/or on the length of the cavity.

When the beam is exactly resonant with the cavity, a π phase-shift will occur between the leaking field and the immediately reflected field, thus cancelling the reflected beam. If the beam is *not* perfectly resonant with the cavity, the reflected beam will no longer cancel.

The expresion in eq.(2.1) is a geometric series, which can be summed up. For the symmetric cavity with no losses, we obtain the reflection coefficient:

$$F(\omega) = \left(\frac{E_{re}}{E_{in}}\right) = \frac{r\left(\exp\left(i\frac{\omega}{\mathrm{FSR}}\right) - 1\right)}{1 - r^2 \exp\left(i\frac{\omega}{\mathrm{FSR}}\right)}, \tag{2.2}$$

where $\mathrm{FSR} = c/2L$ is the free spectral range of the cavity, and the constant c is the speed of light. The real and imaginary part of the reflection coefficient is plotted in figure 3. Notice that the imaginary part of the reflection coefficient provides us with the information about which way to correct the laser, since the value depends on the sign of the detuning from resonance.

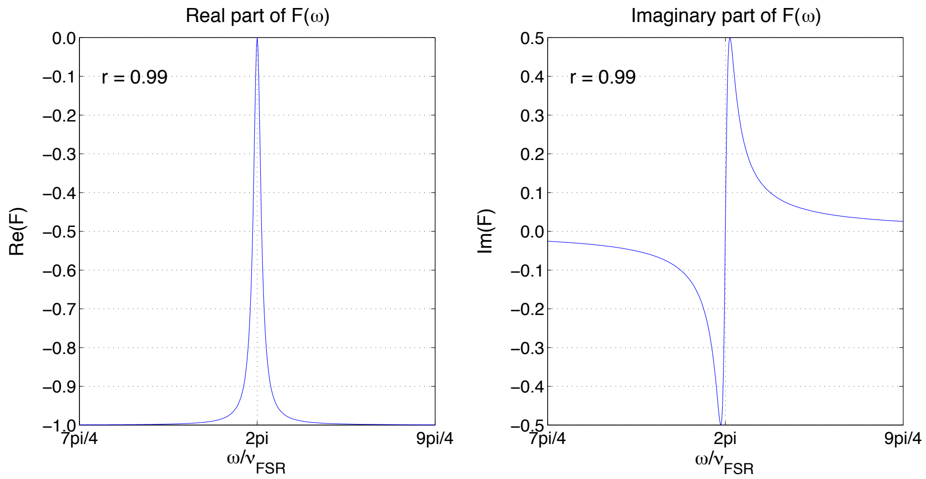

Figure 3: *Real and imaginary part of the reflection coefficient $F(\omega)$. The imaginary part provides us with feedback information used to discriminate between the directions of the detuning from resonance.*

Modulation of incident beam

Our incident beam passes through an electro-optic modulator (EOM) generating *side-bands* on the carrier frequency by modulating the phase of the light, see figure 2. Sidebands are frequency components added to the carrier frequency at an interval of the modulation frequency Ω apart.

An EOM is based on a crystal with the property, that the refractive index is a function of the local electric field. When the crystal is exposed to a local electric field of frequency Ω, the light passing through the crystal will be phase modulated. The modulation will result in first-order side-bands at $\pm\Omega$. Neglecting all other side-bands (of very small amplitude), we get the phase-modulation [7]:

$$E_{in} = E_0 e^{i(\omega t + \beta \sin(\Omega t))} \tag{2.3}$$

$$= E_0 \sum_{n=-\infty}^{\infty} J_n(\beta) e^{i(\omega + n\Omega)t} \tag{2.4}$$

$$\approx E_0 \left(J_0(\beta) e^{i\omega t} + J_1(\beta) e^{i(\omega+\Omega)t} - J_1(\beta) e^{i(\omega-\Omega)t} \right). \tag{2.5}$$

Here we have expanded the expression using Bessel-functions and neglected the higher order terms, while using the relation $J_{-1}(\beta) = -J_1(\beta)$. Our incident light field can be described as three separate beams with frequencies ω and $\omega \pm \Omega$; and amplitudes $J_0(\beta)$ and $J_1(\beta)$. The coefficient β is known as the modulation depth, describing the intensity relation between carrier and side-band frequencies.

The total reflected beam expressed in terms of the reflection coefficient becomes:

$$E_{re} = E_0 \left[F(\omega) J_0(\beta) e^{i\omega t} + F(\omega+\Omega) J_1(\beta) e^{i(\omega+\Omega)t} - F(\omega-\Omega) J_1(\beta) e^{i(\omega-\Omega)t} \right]. \tag{2.6}$$

What we measure, however, is the power incident on a photodiode. Since the reflected power $P_{re} \propto |E_{re}|^2$ the expression becomes:

$$\begin{aligned} P_{re} \propto & |E_{re}|^2 \\ = & P_c|F(\omega)|^2 + P_s\left(|F(\omega+\Omega)|^2 + |F(\omega-\Omega)|^2\right) \\ & + 2\sqrt{P_cP_s}\{\mathrm{Re}\left(F(\omega)F^*(\omega+\Omega) - F(\omega)F^*(\omega-\Omega)\right)\cos(\Omega t) \\ & + \mathrm{Im}\left(F(\omega)F^*(\omega+\Omega) - F(\omega)F^*(\omega-\Omega)\right)\sin(\Omega t)\} \\ & + (2\Omega \text{ terms}). \end{aligned} \tag{2.7}$$

Here P_c and P_s is the carrier and side-band power respectively.

Isolating the $\sin(\Omega)$ term
In eq.(2.7) we are interested in the sine-term oscillating with Ω as it contains information about the imaginary part of $F(\omega)$. This part can be isolated by using a low-pass filter to suppress terms oscillating with frequencies of 2Ω or higher, and then applying a doubly-balanced mixer (DBM) to select the sine-term, see figure 2.

The mixer multiplies two input-signals. From the trigonometric identities, we have the general relation:

$$\sin(\omega_1 t)\sin(\omega_2 t) = \frac{1}{2}\cos[(\omega_1-\omega_2)t] - \frac{1}{2}\cos[(\omega_1+\omega_2)t] \tag{2.8}$$

$$\sin(\omega_1 t)\cos(\omega_2 t) = \frac{1}{2}\sin[(\omega_1-\omega_2)t] + \frac{1}{2}\sin[(\omega_1+\omega_2)t] \tag{2.9}$$

By multiplying the reflected signal of frequency ω_2 with a reference signal of frequency ω_1, the mixer generates signals corresponding to both the sum and the difference of the frequencies of the two input-signals.

If we apply another low-pass filter after the mixer and choose $\omega_1 = \omega_2 = \Omega$ only the $\frac{1}{2}\cos[(\omega_1-\omega_2)t]$ term in eq.(2.8) will survive, since the low-pass filter will extinguish $\cos(2\Omega t)$ and $\sin(2\Omega t)$. We are, in other words, able to select the sine-term in eq.(2.7) by mixing the signal from eq.(2.7) with $\sin(\Omega t)$.

2.1.3 The behaviour of the error-signal

We do not know the reflectivity r of the mirrors in eq.(2.2), so we make a first order approximation of the reflection coefficient $F(\omega)$. If we write $\nu = \nu_0 + \Delta\nu$, we can take advantage of the fact that the ratio between the frequency offset and the resonance frequency $\Delta\nu/\nu_0$ is small compared to the free spectral range. We can approximate the exponentials in eq.(2.2) as:

$$\exp\left(-\frac{2\pi i\nu}{\mathrm{FSR}}\right) \approx 1 - \frac{2\pi i\Delta\nu}{\mathrm{FSR}}. \tag{2.10}$$

This approximation gives us an expression for the reflection coefficient $F(\nu)$ dependent on the FWHM (Full Width at Half Maximum) of the cavity resonance signal $\delta\nu$, rather than the free spectral range and the mirror reflectivity [8, p.272].

$$F(\nu) = -\frac{\Delta\nu(\Delta\nu + i\delta\nu/2)}{(\delta\nu/2)^2 + \Delta\nu^2}. \tag{2.11}$$

Having isolated the terms in eq.(2.7) oscillating with Ω and using eq.(2.11) we can write the reflected power as:

$$P_{re} = b + a[A(\Delta\nu)\cos(\Omega t) + D(\Delta\nu)\sin(\Omega t)], \tag{2.12}$$

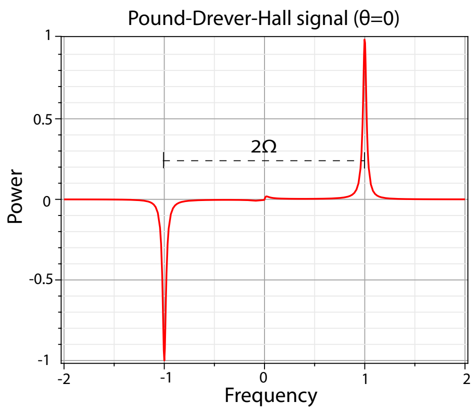

(a) Plot of cosine-dependency $A(\Delta\nu)$.

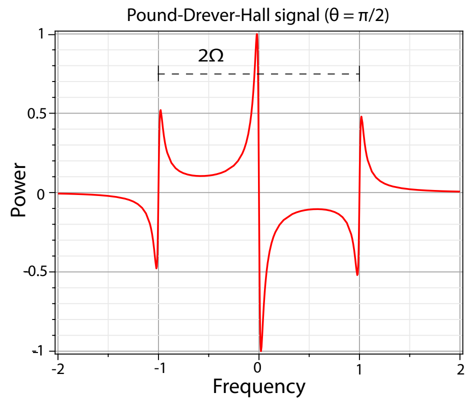

(b) Plot of sine-dependency $D(\Delta\nu)$.

Figure 4: *Plot of the sine $D(\Delta\nu)$ and cosine $A(\Delta\nu)$ terms of P_{re}. The sine term (b) is interesting since it is linear around resonance, and provides us with a sign discriminating between detuning to the right and left of resonance. Ideally this is the signal we want to lock our laser with. The first-order sideband to sideband span (later referred to as the span of the side-bands) of this signal is simply the frequency interval 2Ω.*

where A and D are functions of $\Delta\nu$,

$$D(\Delta\nu) = \frac{-4\Omega^2(\delta\nu/2)\Delta\nu\left[(\delta\nu/2)^2 - \Delta\nu^2 + \Omega^2\right]}{[\Delta\nu^2 + (\delta\nu/2)^2]\left[(\Delta\nu+\Omega)^2 + (\delta\nu/2)^2\right]\left[(\Delta\nu-\Omega)^2 + (\delta\nu/2)^2\right]}, \tag{2.13}$$

$$A(\Delta\nu) = \frac{4\Omega(\delta\nu/2)^2\Delta\nu\left[(\delta\nu/2)^2 + \Delta\nu^2 + \Omega^2\right]}{[\Delta\nu^2 + (\delta\nu/2)^2]\left[(\Delta\nu+\Omega)^2 + (\delta\nu/2)^2\right]\left[(\Delta\nu-\Omega)^2 + (\delta\nu/2)^2\right]}. \tag{2.14}$$

We can investigate the behavior of our signal according to figure 4a and 4b. The ideal shape of our error-signal has only the sine-component of eq.(2.12), see figure 4b, as the curve $D(\Delta\nu)$ will provide information of the frequency offset close to resonance. However, a signal of this pure type is not necessary and we will see later that, in our case, we have a small contribution from the cosine component.

The sine-component is linear close to resonance, which is desirable since the deviation from zero is used as feedback to the laser.

2.2 Noise analysis

It is possible to extract information about the linewidth of our laser and how efficient the feedback lock is by analysing the noise spectrum of the error-signal presented in section 2.1, eq.(2.12).

Correlations between measured data can be expressed by the autocorrelation function. The autocorrelation function for the electric field is:

$$R_E(\tau) \quad = \quad \langle E(t+\tau)E^*(t)\rangle \tag{2.15}$$

where $E(t+\tau)$ is the electric field at the instant $t+\tau$. For totally uncorrelated fields the time average in eq.(2.15) cancels for all possible values of τ and therefore $R_E(\tau) = 0$.

Using the Wiener-Khintchine theorem [8, p.57], one can determine the power spectral density function $S_E(\nu)$ from the autocorrelation function $R_E(\tau)$. The power spectral density describes the power carried by the wave per unit frequency. Intuitively it gives a picture of the frequency components of the wave.

The power spectral density function and the autocorrelation function constitute a Fourier transform pair:

$$S_E(\nu) \quad = \quad \int_{-\infty}^{\infty} \exp(-i2\pi\nu\tau) R_E(\tau) \mathrm{d}\tau. \tag{2.16}$$

If we in eq.(2.16) assume an electric field with frequency fluctuations but negligible amplitude fluctuations and a real amplitude, we arrive at the power spectral density [8, p.65]:

$$S_E(\nu - \nu_0) = E_0^2 \int_{-\infty}^{\infty} \exp[-i2\pi(\nu - \nu_0)\tau] \exp\left(-\int_0^{\infty} \frac{S_\nu(f)}{f^2}[1 - \cos 2\pi\tau] df\right) \mathrm{d}\tau, \tag{2.17}$$

where $S_\nu(f)$ is the power spectral density of frequency fluctuations, and f is the corresponding Fourier frequency.

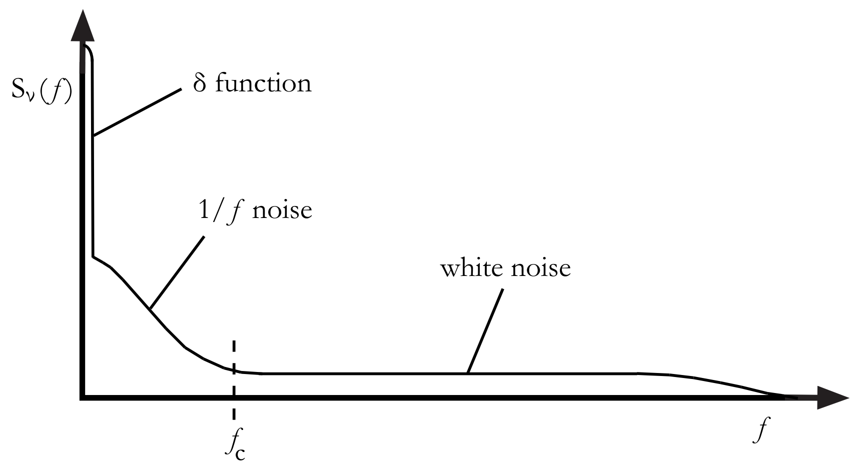

Figure 5: *Conceptual model of the power spectral density showing the corner frequency f_c between the $1/f$ and white noise regimes. Because of energy-conservation, the power spectral density must go to zero at high frequencies.*

Figure 5 shows a conceptual model of the power spectral density S_ν. Three characteristic areas are shown, indicating the typical behaviour of the noise. The δ-function near zero shows up when the signal fluctuations have a non-vanishing mean, corresponding to a DC-offset of the signal. The $1/f$-dependency typically stems from technical noise, such as electrical carrier fluctuations [9, 10]. The power spectral density becomes independent of the frequency in the white noise regime, and must finally go to zero at high frequencies, for reasons of energy conservation.

Generally the power spectral density can be reasonably well modelled [8, p.58] by a superposition of five independent noise contributions, of which three have been mentioned above. They each obey a power law, with integers $-2 \leq \alpha \leq 2$:

$$S_\nu(f) = \nu_0^2 \sum_{\alpha=-2}^{2} h_\alpha f^\alpha, \tag{2.18}$$

where ν_0 corresponds to the centre laser frequency, and h_α is a coefficient giving the weighting of the particular noise type. We have that $\alpha = -2$ corresponds to a random walk of frequency noise often caused by the surrounding environment, such as changes in temperature and vibrations. Flicker frequency noise observed in active devices (such as our diode laser) follows the $\alpha = -1$ behaviour, and the $\alpha = 0$ behaviour is white frequency noise. The positive values for α are flicker phase noise and white phase noise corresponding to $\alpha = 1$ and $\alpha = 2$ respectively.

2.2.1 Laser lineshape

The lineshape of the laser in general has a Voigt profile [11]. The Voigt profile is a convolution between the Lorentzian and Gaussian distribution, and thus the profile of the laser can be approximated as either Lorentzian or Gaussian, depending on the power spectral density profile.

From the ratio $S_\nu(f_c)/f_c$ one can determine how to best approximate the lineshape [8, p.67]:

$$S_\nu(f_c)/f_c \gg 1 \quad \rightarrow \text{Lorentzian} \tag{2.19}$$

$$S_\nu(f_c)/f_c \ll 1 \quad \rightarrow \text{Gaussian.} \tag{2.20}$$

Here, f_c is the corner frequency above which the white noise dominates, see figure 5. The Lorentzian lineshape generally originates from spontaneous emission in the laser diode, whereas statistical fluctuations of charge-carriers in the laser causes a Gaussian lineshape. This Gaussian can be thought of as the result of the Lorentzian fluctuating about a central frequency [11].

Lorentzian power spectral distribution

If we interpret our signal as having only white frequency noise S_ν^0, and thus concentrate on Fourier frequencies above the corner frequency f_c of figure 5, the scenario of eq.(2.19) becomes a very good approximation. This scenario is relevant for very short timescales, where the fequencies below f_c are no longer of interest. Performing the integration in eq.(2.17) leads to:

$$S_E(\nu - \nu_0) = 2E_0^2 \frac{\gamma/2}{(\gamma/2)^2 + 4\pi^2(\nu - \nu_0)^2}, \tag{2.21}$$

where $\gamma = 2\pi(\pi S_\nu^0)$. The power spectral density of the electric field given in eq.(2.21) is a Lorentzian distribution with full width half maximum:

$$\Delta\nu_{\mathrm{FWHM}} = \pi S_\nu^0. \tag{2.22}$$

So by determining the value of the white noise floor S_ν^0, one can estimate the Lorentzian linewidth of the laser.

Gaussian power spectral distribution

For signals with a more prominent $1/f$-part of the noise spectrum, the linewidth can no longer be represented by a Lorentzian. Here, eq.(2.20) will be the proper approximation. The linewidth for the Gaussian lineshape can be computed as the mean frequency excursion:

$$\Delta\nu_{\rm rms} = \sqrt{\int_{1/T}^{f_c} S_\nu(f)\mathrm{d}f}, \tag{2.23}$$

where T is the measurement time defining the lowest measurable Fourier frequency in the spectrum. If the power spectral density has been measured we can estimate the linewidth by numerical integration of the obtained curve up to the corner frequency f_c.

In section 4.2.6 we compute both these linewidths, as our power spectral density does not belong to either of the extremes in eq.(2.19) and (2.20). But first we will take a look at the experimental setup.

3 Setup

A large part of our project has consisted in building the actual PDH-system. This system is used to lock the laser to a cavity-resonance, and thus eliminate some of the coarse noise of the laser frequency. Our system intentionally uses a low-finesse cavity, which will give us a large capture range for the locking of the laser frequency compared to a high-finesse cavity. Hereby we greatly increase the ease with which we can lock our laser to the high-finesse PDH-system. In figure 6 an overview of our low-finesse PDH setup is shown. In the following sections we detail the essentials of the system and discuss some of the considerations we made in the process of setting up the system.

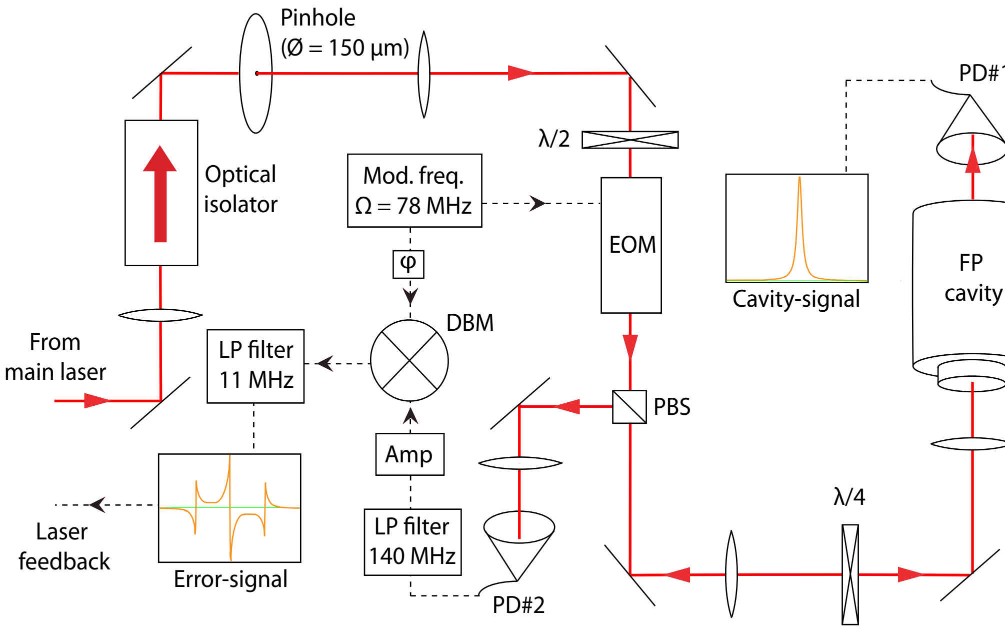

Figure 6: *Setup of laser system. Red lines indicate laser light, and dashed lines indicate electrical signals. The reflected light from our Fabry-Perot Cavity (FP) is directed towards a separate photodiode (PD#2) via a polarizing beam splitter (PBS), and here manipulated into the error-signal we seek. EOM is the Electro-Optic Modulator, $\lambda/2$ and $\lambda/4$ are retarder-plates controlling the polarization of the beam, and enabling us to separate the reflected cavity-signal.*

3.1 Overview

From the main laser a small fraction of the light is split off and directed towards our setup. The light is oscillating in a single mode, at a wavelength of 914 nm. Firstly, the light passes through an optical isolator, a pinhole and a $\lambda/2$-plate ensuring that we minimize the optical feedback, and have control over the shape and polarization of our beam. We then modulate the phase, by passing the light through an EOM, generating side-bands at a frequency-offset of $\pm\Omega$, where Ω is the modulation frequency. In order to isolate the carrier and first order side-band frequencies, we choose $\Omega = 78$ MHz. The light is then sent to a cavity with the front mirror mounted on a piezo crystal. The piezo allows us to change the length of the cavity and thus scan over an interval of resonance-frequencies.

The reflected signal is directed onto the second photodiode (PD#2) by means of a polarizing beam splitter (PBS) followed by a $\lambda/4$-plate. The linearly polarized light incident on the EOM is converted to circularly polarized light by the $\lambda/4$-plate. Upon reflection the light travelling back from the Fabry-Perot cavity is converted to the orthogonally linear polarization mode with respect to the incoming light. This makes it possible for the PBS to divert the reflected part of the light without inflicting the incoming light.

The reflected light will have a profile E_{re} as described in section 2.1 when incident on the photodiode (PD#2). Passing the electrical output signal through a low-pass filter with a cut-off frequency of 140 MHz, we remove the part of the signal stemming from higher-order side-bands. After amplifying this signal, we mix it with our modulation signal to obtain components oscillating with the sum and the difference of the two frequencies. Via another low-pass filter (at 11 MHz) we isolate the difference signal, obtaining the error-signal we can use as a locking-signal. A feedback loop finally regulates the main laser current, and consequently its frequency.

3.2 Considerations

In the overview above, the essential parts of the PDH-scheme are mentioned and their functions explained. While these are essential to the system, they do not constitute the complete setup. A number of considerations has to be made in order to obtain the optimal form of the laser-beam.

Beam shape

It is important that the beam has the optimal shape, that is, it needs to be Gaussian and adapted correctly to our Fabry-Perot interferometer, i.e., have the right beam waist, and a curvature matching the curvature of the mirrors. Pinhole and lenses are implemented in order to improve and control the Gaussian shape of our beam.

The first lens focuses the beam at the pinhole, and by choosing a pinhole slightly smaller than the beam waist, we ensure that our beam is nice and Gaussian without losing too much power.

The following three lenses are all implemented in order to regulate the position of the beam-waist as well as the Rayleigh-range, ensuring that we can properly couple light into our Fabry-Perot cavity. To keep the signal to noise ratio as high as possible and for power reasons, the reflected beam is also focused onto the photodiode (PD#2) with a lens.

Beam trajectory

Mirrors are needed for several practical reasons; they are used to navigate the laser beam and reduce the physical size of the setup, but also to allow a correct incidence on the photodiodes, the pinhole and, most important of all, on the cavity.

While elements like the PBS, EOM, retarder-plates and lenses are not very sensitive with respect to the beam trajectory, our pinhole and cavity are very much so. Here the two mirrors are essential as they allow us to steer both the direction and the origin of the beam, in terms of incidence on the second mirror.

Cavity length

As mentioned above, the front cavity-mirror is mounted with a piezo, allowing us to scan over several resonance frequencies by modulating the length of the cavity. This greatly improves the ease of adjusting mirrors and lenses to obtain the correct resonant mode. It also provides us with an easy method of producing plots of the error-signal as well as the signal of resonance in the cavity, recorded with PD#1, see figure 7. When locking the laser signal we do not scan the length of the cavity, but use the piezo to adjust our cavity length to any desired resonance frequency.

Modulation frequency Ω
The EOM generating side-bands is set to a specific frequency Ω chosen to optimize our setup. It is important that this frequency is not too low, in order to properly be able to discriminate between the carrier signal and the side-bands, thus arriving at the correct error-signal.

Most of our measurements have been made with a modulation frequency of $\Omega = 78\,\text{MHz}$, giving side-bands just on the shoulders of the carrier Lorentz-shape. Throughout we have used the same phase-relation between modulation signal and reflected signal, adjusted by a delay line rather than an actual phase-modifying component as in figure 6. This provides a robust error-signal with the characteristic shape of figure 4b.

Later on, measurements were made with a modulation frequency of $\Omega = 98\,\text{MHz}$, in order to more efficiently extinguish the higher order side-bands with our first low-pass filter. This provided no disadvantages with respect to the error-signal shape, and could well have been implemented earlier on, had we wished to do so.

Optical isolator
Finally, an optical isolator is introduced in the beginning of our system in order to minimize the optical feedback generated by reflections interfering with the main laser. Every element in our setup will cause reflections, and if the incidence of the laser beam is normal to the surface of the element, reflections will follow the exact same path back. If they reach the main laser, their interaction with it will cause a very noisy laser signal in our whole system.

4 Results

In this section we will present some of the results obtained from analysing our data. The first section will concentrate on characterizing our cavity and providing experimental confirmation of some of the above theory.

Our system enables us to stabilize the input laser by locking it to the resonance frequency of the cavity. Characterizing the efficiency of this lock will constitute the second part of this section (4.2), providing us with a characterization of the signal noise as well as the laser linewidth.

4.1 Pound-Drever-Hall stabilization of the laser

4.1.1 Measurements

As seen from the setup in figure 6, we have two measurement points in our system (shown as small yellow graphs). One is positioned after the mixing system following the photodiode that receives the reflected signal (PD#2), as described in section 3. This measurement point provides us with the error-signal we use for locking the laser-frequency.

The other measurement point is positioned at the photodiode (PD#1) directly after our cavity and provides us with a resonance-signal (later referred to as the cavity signal). This signal is simply used to align the system properly and to characterize our cavity.

We wish to scan the frequency domain, and rather than trying to change the laser frequency directly, we make use of the piezo-mounted mirror on the cavity front. With this piezo, we can scan over a *length-interval* of the cavity. Changing the length of the cavity L changes the resonance frequency ν_0 and will provide us with a picture corresponding very neatly to a scan over frequencies,

$$\nu_0 = \frac{c}{2L} \quad \xRightarrow{\text{To first order}} \quad \frac{\delta L}{L} = \frac{\delta \nu}{\nu_0}. \tag{4.1}$$

The scan-signal is a triangle-wave modulation at approximately 60 Hz, enabling us to have one or two full error-signals in one scan cycle.

Our raw data is measured in time versus voltage, as seen on figure 7. Since we applied a triangle-wave to the piezo crystal, see figure 7c,, the time is directly proportional to the voltage, and thus the cavity length.

4.1.2 Calibration

As explained in section 2.1 our EOM modulation frequency Ω generating side-bands on the laser frequency results in a characteristic span of the first-order side-bands, see figure 4b. The offset from carrier-frequency to first-order side-bands is Ω in the frequency domain, hence we know that the frequency-difference in the error-signal between the two side-bands is $2\Omega = 156\,\text{MHz}$.

This knowledge provides us with a conversion factor between time and frequency, where the time is proportional to a given voltage of the piezo, or length of the cavity.

Non-linearity of frequency scan

When measuring the span of the side-bands of our error-signal, as displayed in figure 4b, we see that the span varies with time t. In order to distinguish between this span and our known value 2Ω, we label the measured span of the side-bands 2Δ, where $[\Delta] = \text{s}$. We obtain values for 2Δ in the range 0.584 ms to 0.808 ms by fitting to the error-signals, see section 4.1.3. A scan-period lasts for approximately 8 ms.

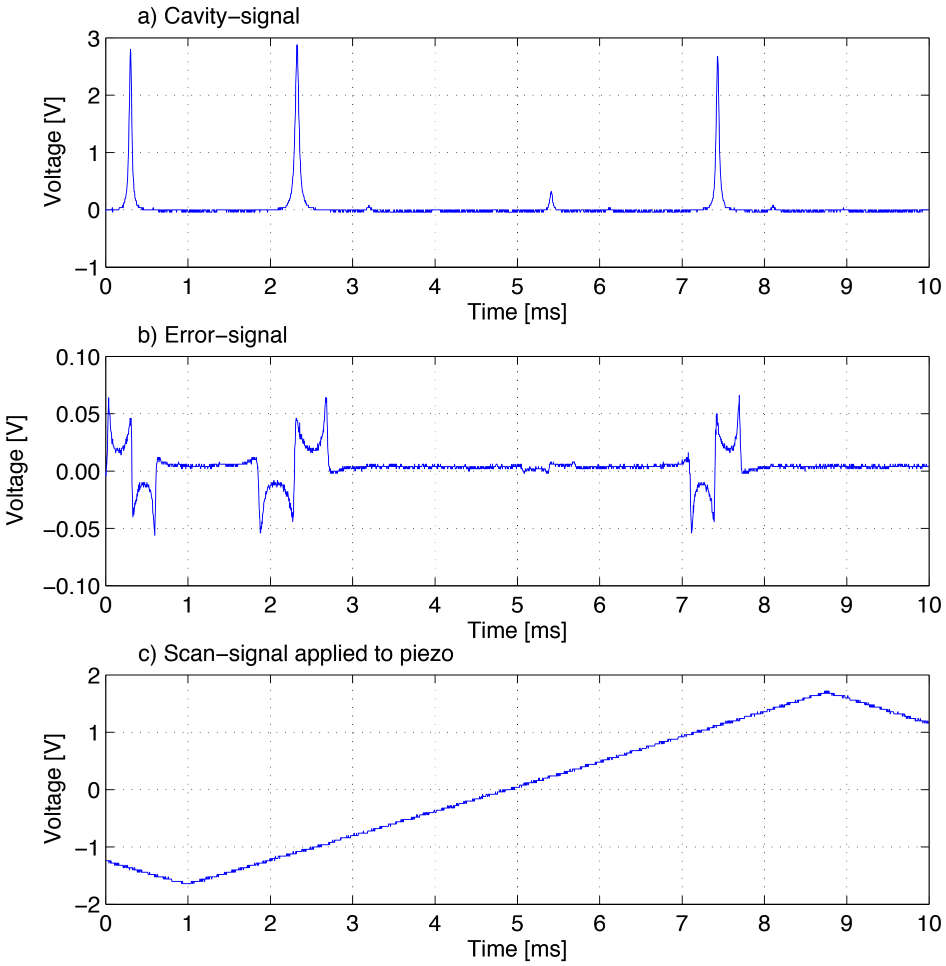

Figure 7: *Plot of measured cavity-signal, error-signal and scan-signal from oscilloscope. With reference to figure 6, figure 7a) is obtained by measurement with PD#1, and figure 7b) with PD#2. The scan-signal in figure 7c) is obtained by connecting the frequency-generator directly to the oscilloscope. The signal of figure 7c) is applied to the piezo thereby changing the cavity length and thus scanning over resonance frequencies. This gives rise to the signals in figure 7a) and 7b) showing us the cavity resonances and the corresponding error-signals, respectively. Notice the difference in the span of the side-bands of the error-signal depending on time, which is proportional to the scan-signal voltage.*

If the frequency scaled linearly with time then the measured span of the side-bands would be constant: $2\Delta = \text{constant} \cdot 2\Omega$, because all the datasets are modulated with the same frequency $\Omega = 78\,\text{MHz}$. Since this is not the case, it seems that the conversion between time and frequency is non-linear.

Calibrating the frequency axis

From each measured span of the side-bands in the error-signals, we can compute a stepsize $s = \Omega/\Delta$ relating an interval of scanning-time to an interval of frequency. Due to the non-linearity this stepsize will be dependent on where in the scan-period we are, and thus seen as time-dependent.

In figure 8 the calibration stepsize s as a function of time t is plotted together with a fit to s. We have used a power-function for the fit, since a plot of Δ versus time t on a double logarithmic plot exhibits a linear trend.

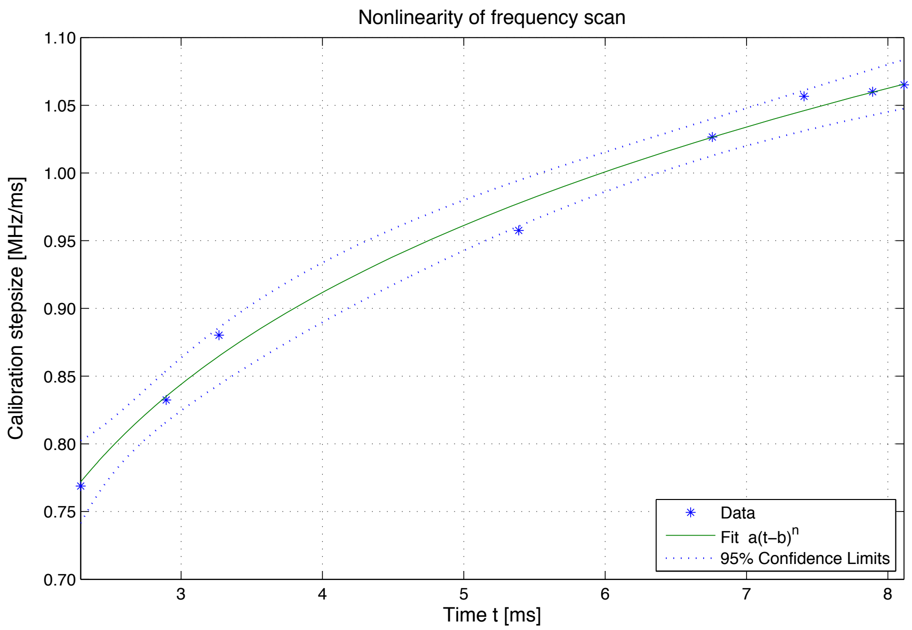

Figure 8: *Calibration curve for the frequency axis, showing* 95% *confidence limits of the fitted curve. The datapoints are obtained by noting the span of the side-bands* Δ *as a function of time, and thus piezo voltage, see scan-signal in figure 7b. The calibration stepsize is* Δ/Ω. *The fitted values of the coefficients are:* $a = 0.77\,MHz/ms^{n+1}, n = 0.17, b = 1.26\,ms$.

The fitted stepsize function $s(t)$ in figure 8 allows us to deconvolute the time-axis of our datasets and convert the time-axis to frequency. We cannot determine an absolute zero-point for the frequency axis, but the frequency intervals will have the right size, which is all we are concerned with.

Origin of the non-linearity

A first guess as to the origin of the non-linearity of the scan could be the piezo crystal used to scan the cavity. When a piezo crystal is exposed to high voltage it can change length in a way which is not entirely linearly dependent on the voltage. This can be due to the structure of the piezo crystal itself or, for instance, due to the glue used between the piezo and the cavity-mirror.

4.1.3 Cavity FWHM from error-signal

The error-signal is generated from the light reflected off the cavity as described in section 2.1. The error-signal controls the feedback loop, used to stabilize our laser, but in order to analyse it properly we split some of the signal off to an oscilloscope. What we observe on the oscilloscope is a voltage-readout as a function of time. We modulate the piezo, and thus the length of the cavity, and make use of the conversion given in eq.(4.1).

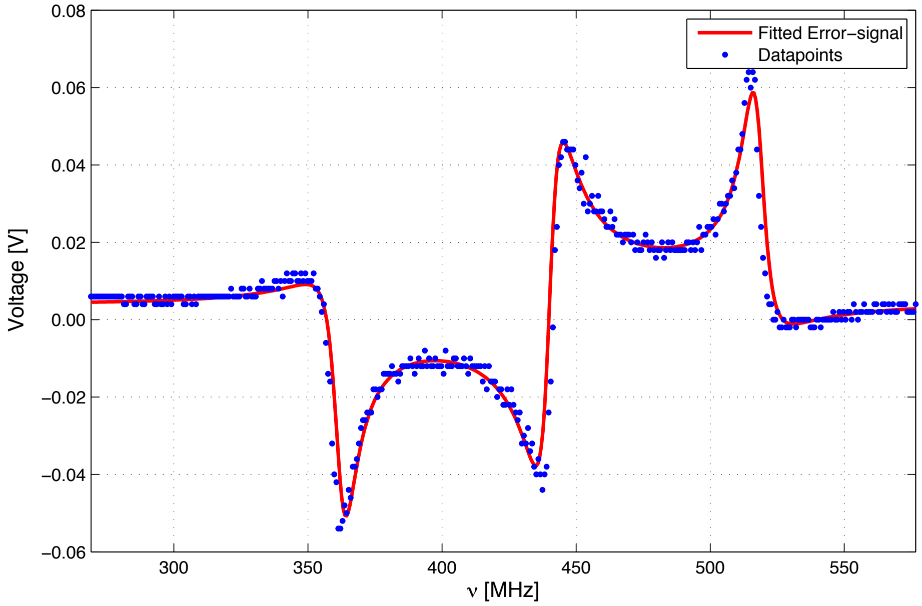

Figure 9: *Example of fitted error-signal. The small fit-interval minimizes distortion errors due to the non-linearity of the frequency-axis. The error-signal is not the pure sine-term of eq.*(2.7) *we see in figure 4b, but also contains a small part of the cosine-component* $A(\Delta\nu)$*, see figure 4a. The fit yields a FWHM of* 10.2 *MHz with a fit uncertainty of* $\sim 100\,kHz$*.*

Fitting to the error-signal

We wish to fit eq.(2.12) to our error-signals, in order to determine the characteristic FWHM of the cavity resonance, see figure 9. To do this we use only a small portion of the dataset, zooming in on a single error-signal. We do this for several reasons:

Firstly, some of our datasets have multiple visible error-signals, but only one or two that is fully visible, making them a candidate for fitting. Other datasets will include error-signals from the second half of the scan-period. These error-signals are mirrored, and will once again result in poor fitting. Both of these instances is represented by the error-signal to the far left on figure 7b.

Secondly, our time-axis does not scale linearly with frequency, and consequently a smaller fit-interval results in less distortion. The fitted values of the span of the side-bands in the error-signals are used to produce the calibration curve in figure 8.

In section 2.1.3 we concluded that the pure sine-component $D(\Delta\nu)$ of eq.(2.12) would be the ideal error-signal, see figure 4. We also mentioned that it was no necessity. The signals we have obtained are all similar to figure 9 with respect to the sine vs cosine-dependency on the phase θ. Here, we are not dealing with a perfect sine-component but rather a mixture of the sine and cosine components. This results in the peaks close to resonance becoming smaller than the other peaks. For a very accurate lock, the linear part of the error-signal near resonance needs to be as steep as possible. Having a pure sine-component ensures this. In our case, however, the efforts needed to adjust the phase θ to yield only a sine component, do not match the benefits of a better accuracy.

A few datasets were discarded due to severe voltage fluctuations and distorted proportions. The voltage fluctuations these error-signals exhibited, could be caused by acoustic noise, whereas laser-drift could distort the proportions of the error-function, ruining the symmetry of the error-signal with respect to the carrier-frequency.

4.1.4 Cavity FWHM from cavity-signal

The part of the laser-light that propagates through our cavity will have increased intensity around cavity resonance. This results in a signal with resonance peaks, an interval of the free spectral range (FSR) apart. In section 4.1.2 we found that there is a non-linearity of the time-axis, making it insufficient to simply measure this interval directly. By characterizing the non-linearity though, we are able to find the FSR, and this will be done i section 4.1.5. In this section we will investigate the resonance peaks themselves, and obtain a value of their FWHM from fitting a Lorentzian curve to the data, see figure 10.

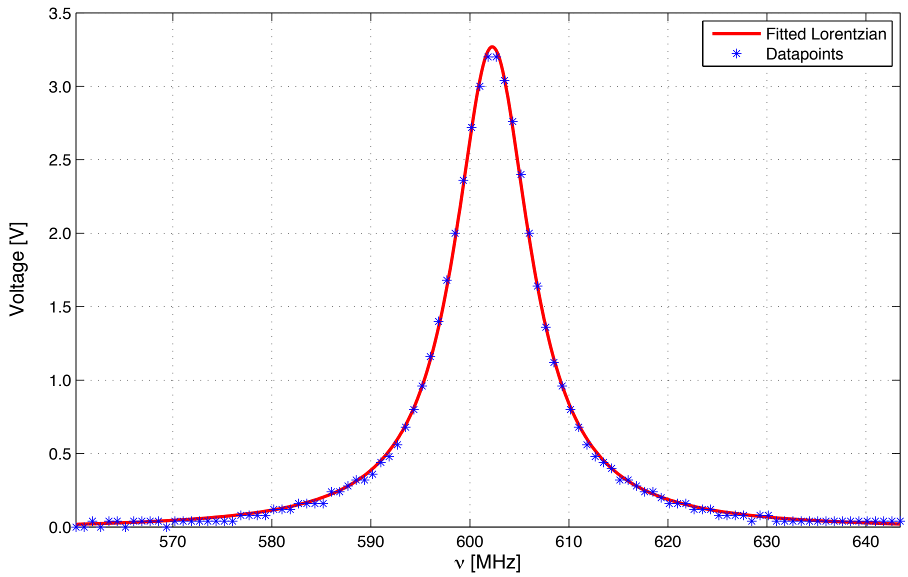

Figure 10: *Example of a Lorentz-fit to a resonance peak. The side-bands added to the laser signal by the EOM are not visible as they are outside the frequency range. The fit yields FWHM* $= 9.2\,MHz$ *with a fit uncertainty of* $\sim 100\,kHz$.

In figure 10, we only see the resonant carrier-frequency of our laser signal, as the side-bands expected at approximately 680 MHz and 436 MHz are out of range. Furthermore the intensity of the side-bands are too low for the oscilloscope to resolve them at this gain setting.

One of the fit parameters of a Lorentzian is the FWHM, and we readily obtain values for each dataset. Similar to the treatment of the error-signal, we only fit to a small interval in the vicinity of the resonance peak. Each resonance peak has a corresponding error-signal, see figure 7, and the stepsize s calculated from this error-signal is used to transform the time-axis to frequency units.

The FWHM obtained from the cavity-signal can be seen in figure 11 plotted together with the FWHM obtained from the error-signal. The green errorbars are the fit-uncertainties from the fit to the error-signal. The blue errorbars results from the fit-uncertainties to the cavity-signal and from the propagated uncertainties of the stepsizes. The weighted mean and standard deviation of the weighted mean are also displayed on the figure.

The weightings used are from the fitting uncertainties. We obtain a weighted mean:

$$\text{FWHM} = (9.7 \pm 0.1)\,\text{MHz}. \tag{4.2}$$

The linewidth of the laser does not contribute significantly to our measurements of the cavity FWHM. For the measured FWHM we have:

$$\delta\text{FWHM} = \sqrt{\delta\nu_{cavity}^2 + \delta\nu_{laser}^2}. \tag{4.3}$$

But the contribution of the laser is very small, since $\delta\nu_{cavity} \sim 1\,\text{MHz}$ and $\delta\nu_{laser} \sim 10\,\text{kHz}$.

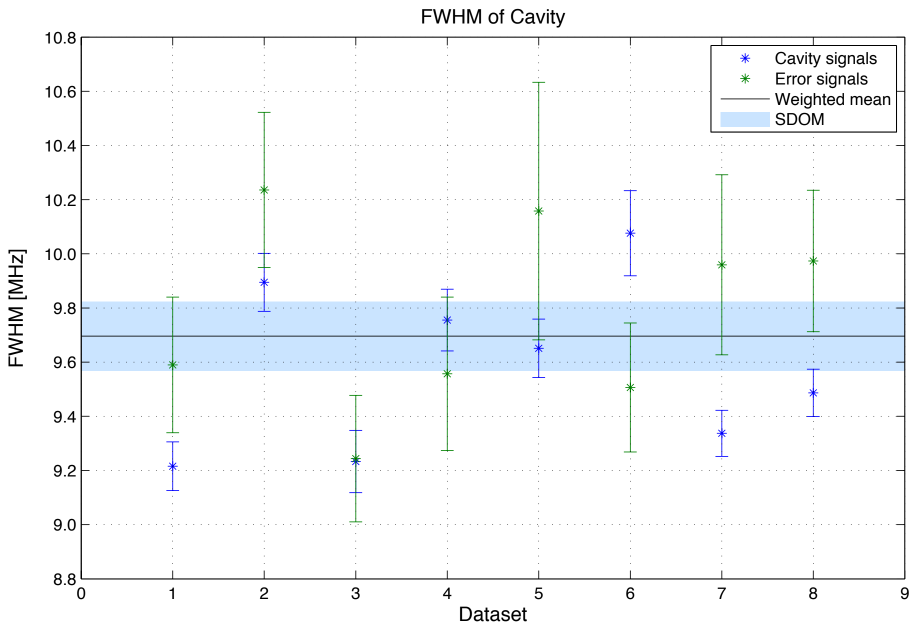

Figure 11: *FWHM obtained from both error- and cavity-signal. This is the linewidth of our cavity. Error-bars display fit uncertainties, whereas the light blue area visualizes the standard deviation of the mean (SDOM).*

4.1.5 Free Spectral Range

The calibrated frequency axis allows us to determine the free spectral range (FSR) by simply calculating the distance in frequency between the centre of two error-signals in a dataset. If the centre of the first error-signal is denoted t_1 and the centre of the second error-signal is denoted t_2 we have:

$$\text{FSR} = \int_{t_1}^{t_2} s(t)\ \mathrm{d}t, \tag{4.4}$$

where $s(t)$ is the fitted step-size function shown in figure 8. The interpretation of eq.(4.4) is as follows: Each infinitesimal time-step is multiplied by the step-size in that particular point. We sum them all up to obtain the interval in units of frequency.

Using eq.(4.4) we get the FSR values displayed in figure 12. We have 3 datasets each containing 2 error-signals, and thus 3 values of the FSR. The error propagated from fit-uncertainties to the error-signal and in the fit to $s(t)$ turns out to be much smaller than the standard deviation (SD) of the three calculated FSR values, and they are all within the data points. We therefore use the SD of the three FSR values to calculate the standard deviation of the mean (SDOM). Our result becomes:

$$\text{FSR} = (1201 \pm 6)\,\text{MHz}. \tag{4.5}$$

If we used the propagated uncertainties instead, figure 12 could indicate a systematic error. Temperature fluctuations could cause a drift of the FSR, but since the datasets are recorded within 30 minutes and the expansion of the cavity Zerodur to first order gives rise to a frequency change of less than 1 kHz for a temperature change of 0.1 K, this explanation does not seem reasonable.

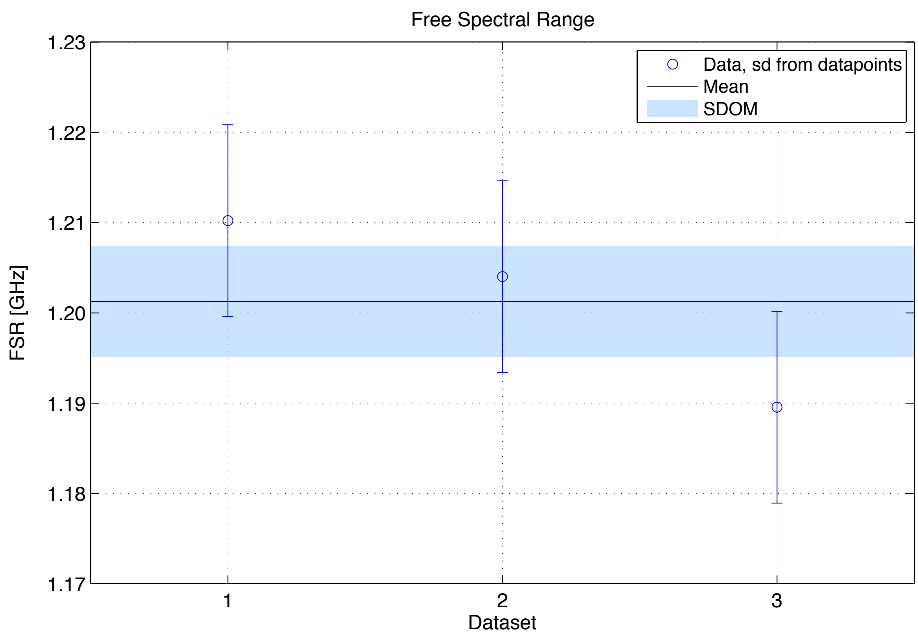

Figure 12: *Free spectral range (FSR) values of our cavity. By utilizing the calibration for the non-linearity of our frequency-scan found in section 4.1.2, we obtain a value of the free spectral.*

4.1.6 Cavity finesse and length

We have now obtained values of our cavity FWHM at resonance and the cavity FSR. This allows us to calculate the finesse $\mathcal{F}$ as well as the length L of the cavity. We are dealing with a low-finesse cavity, as this was an essential part of the idea of using our PDH-setup to pre-stabilize the laser. We also have a measure for the length of the cavity obtained from mirror-specifications and simple measurement with callipers.

The cavity finesse and length are calculated from the above values as follows:

$$\mathcal{F} = \frac{\mathrm{FSR}}{\mathrm{FWHM}}, \tag{4.6}$$

$$L = \frac{c}{2}\frac{1}{\mathrm{FSR}}. \tag{4.7}$$

Using the weighted mean of our FWHM-value in figure 11, we obtain the finesse:

$$\mathcal{F} = 124 \pm 2.$$

The measured length of our cavity is found by calculating the distance between the two coated mirror-surfaces. This has been done by taking into account the length of the glass rod separating them, the (neutral) piezo length and the curvatures of the mirrors. We arrive at a length $L_{\mathrm{measured}} = (124.7 \pm 0.1)\,\mathrm{mm}$ which we compare to our data $L_{\mathrm{data}} = (124.8 \pm 0.6)\,\mathrm{mm}$ and obtain:

$$L_{\mathrm{data}} - L_{\mathrm{measured}} = (1.1 \pm 0.7)\,\mathrm{mm}.$$

The difference observed here could be explained by glue on the mirror surfaces and the piezo.

4.2 Linewidth of the stabilized laser

Ideally our laser would be oscillating at only one frequency ($\sim 328\,\mathrm{THz}$). However, in reality this will not be the case, and many factors can contribute to *noise* in the frequency. Noise is basically any unwanted oscillations of the laser frequency in time, and can result from thermal, acoustic or electromagnetic disturbances of the system.

We use a Fast-Fourier-Transform spectrum analyser (FFT) to record a noise spectrum. An FFT has an implemented algorithm that allows it to calculate a spectrum corresponding closely to the Fourier-transform of the signal, in a very short time. Using this apparatus, we can construct a Fourier-spectrum with detailed information about the distribution of frequencies in our voltage signals. The signal generally has the characteristic shape shown in figure 5, with a $1/f$ dependency followed by a white noise floor. The frequencies of interest here are extremely low compared to our laser frequency. We modulate our signal at 78 MHz in order to obtain the error-signal described in section 4.1 and even this modulation frequency is too far out in the white noise regime to be visible in our spectra.

When analysing a signal the different frequencies that appear in our Fourier-spectrum are denoted Fourier-frequencies. They are the sinusoidal components that constitute the total signal, and not to be confused with what we denote as the frequency of the laser.

The Fourier-frequencies which we will look at in the following are all in the range of a few Hz to $\sim 10\,\mathrm{kHz}$. This range will only just allow us to see the level of the white frequency noise but is chosen out of technical considerations. We demand a certain resolution of the FFT in order to resolve the details in the obtained spectra, and this limits the range of frequencies to a maximum of $\sim 10\,\mathrm{kHz}$. But since the information we are interested in is contained within the interval of Hz to $\sim 10\,\mathrm{kHz}$ it is not a problem.

By utilizing what we have presented in section 2.2.1 we will determine the linewidth of the laser in this section. This is done with and without employing our feedback loop, thus providing us with an estimate of the efficiency of our lock. Furthermore, the Fourier-spectra will allow us to characterize the noise, pointing us in the direction of any sources of noise that it might be possible to eliminate.

4.2.1 Measurements

The error-signal is coupled to the FFT to obtain our noise spectrum. From the setup in figure 6 it is seen that if we measure the error-signal, it is not just the noise of the laser frequency we measure. We will be measuring all of the effects from the the electrical components added to the laser noise.

We are interested in obtaining the power spectral density (PSD) of our signal. By measuring at this point, any noise added by the electrical components will constitute a part of the feedback signal. This enables us to compare the noise of the total signal with the noise of the electrical components alone. Measuring with no light incident on the photodiode (PD#2) will provide us with an estimate of the noise from the electrical components alone. A similar measurement, but this time *with* the laser light, though tuned far off resonance, incident on the photodiode, will provide us with an estimate of shot-noise effects. The FFT measures in units [V^2/Hz] which constitutes a measure of power per frequency interval, since power is proportional to the square of the electric field.

The bandwidth of the FFT determines the frequency bin size, and thus the smallest frequency that can be resolved by the FFT. With the resolution of figures 14 and 15 our FFT bandwidth was 30.6 Hz.

4.2.2 Calibration

As we are interested in the PSD of frequency fluctuations and would like to be able to obtain a measure of the laser linewidth, we wish to have the PSD in units of [Hz^2/Hz]. Having these units we will effectively get the value of the white noise floor in [Hz]. As the FFT measures in units of [V^2/Hz], we use information from the error-signal to obtain a conversion factor C.

Close to resonance the error-signal is approximately linear, as displayed in figure 13. The slope of the error-signal, provides the conversion factor C with units of [V/Hz], and thus allows us to calibrate the PSD by multiplying our data points of units [V^2/Hz] with $1/C^2$.

4.2.3 Power spectral density for $\Omega = 78\,\mathrm{MHz}$

In figure 14 the PSD of our laser modulated with 78 MHz is displayed for four different scenarios.

The green curve represents the noise of the free-running laser. We tune the cavity manually to resonance with the laser, so that the drift of the laser frequency will not distort the spectrum. In this situation we expect to find the largest amount of noise in our system.

The light blue curve is the electrical noise of the system, when the photo diode (PD#2) is blocked with a piece of paper. We are effectively measuring the background noise of the electrical components, providing us with a minimum level for the noise, and a minimum level for how well we can lock the laser frequency.

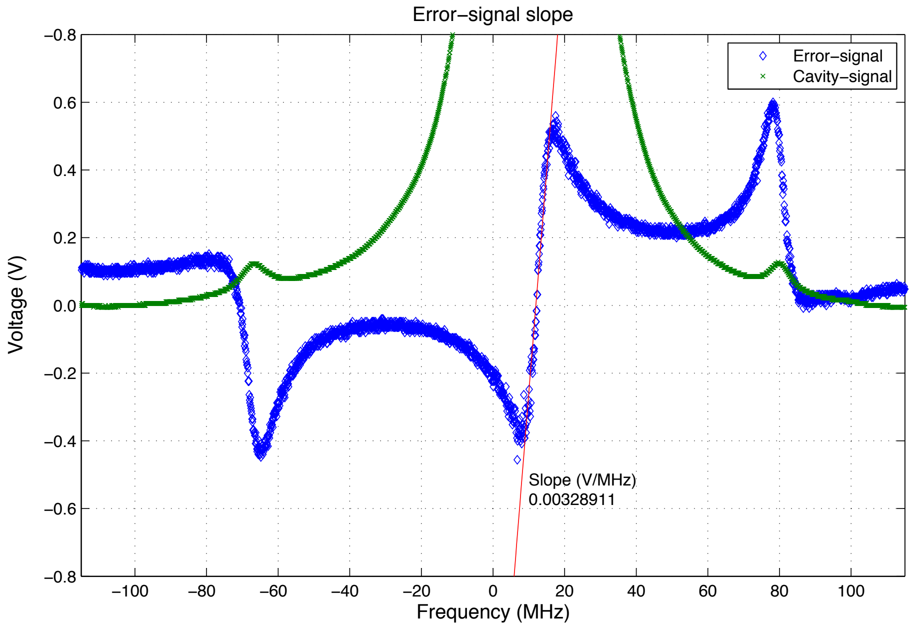

Figure 13: *Plot of the error-signal and the cavity-signal for $\Omega = 78$ MHz. The slope C of the error-signal is used for calibration of the noise spectrum. Here the side-bands at ± 78 MHz with respect to resonance frequency are visible on the cavity resonance-signal.*

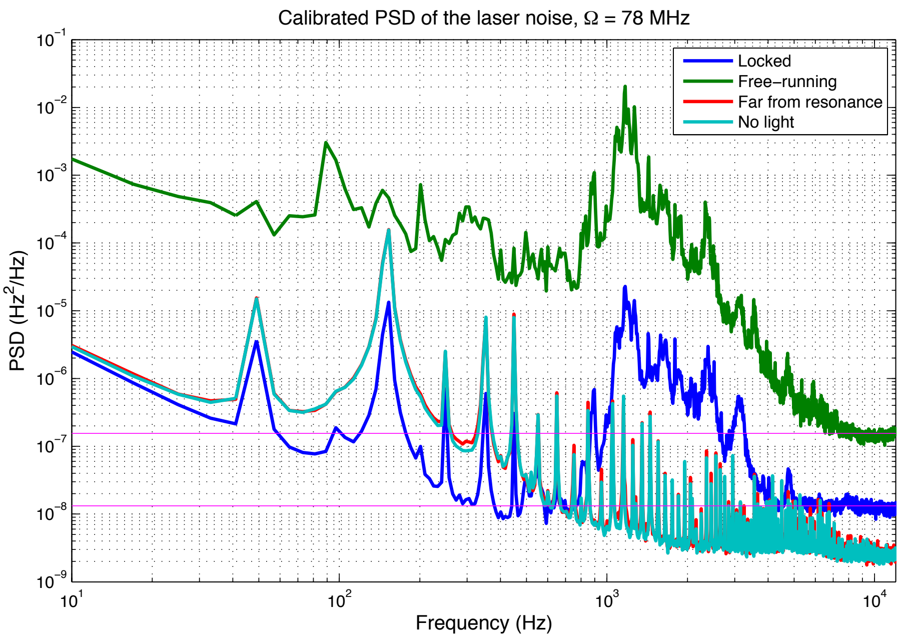

Figure 14: *Power spectral density of noise for $\Omega = 78$ MHz. FFT Bandwidth: 30.6 Hz. Horizontal lines indicate white noise floors used for the calculation of Lorentzian linewidth.*

The red curve is the noise when the laser is far from resonance with the cavity, and is barely visible in figure 14. There will be no error-signal here, and so this is done solely to estimate whether the statistical fluctuations of photons, the shot noise, have an influence on our spectrum. If the shot-noise from the photodiode were larger than the background noise of the system, the red curve would contain more noise than the light blue. This, however, is not the case. The level of the shot-noise is less than the background noise, and both the red and light blue curve represent the background noise of the system.

The dark blue curve is the noise of our system when the laser is locked. Here, the laser frequency is on resonance with the cavity, and the error-signal now provides a feedback locking measure. As expected, this situation contains less noise than in the case of the free-running laser, but the background noise seems to exceed the dark blue curve in the frequency interval of $10 - 600\,\mathrm{Hz}$. This is unphysical because, as explained above, we know that the noise level of the locked laser will not be able to pass under the noise level of the background. When operating, the feedback lock receiving the error-signal tries to correct any unwanted drift of the signal. Basically any noise in the signal is interpreted as a drift away from the error-signal-resonance at zero voltage. Now if the laser did *not* have any noise, no correction would be needed. However, the error signal will still be a superposition of the background noise of the electrical components and the error-signal. This signal will demand a feedback signal to the laser though no correction is needed, and thus noise will be *written* onto the laser signal.

Figure 14 shows the locked-laser signal noise as being *less* than the background noise for low frequencies. This evidently means that the noise written onto the laser frequency in the above described process cancels out some of the inherent background noise of the system. It is important to notice that the laser is not less noisy than the background, it merely looks as though this is the case due to the noise written onto the laser frequency. While this is our suspicion, we have not attempted to correct for it in our calculations. This omission is due to the problem of properly evaluating the true noise.

In section 4.2.5 we will look closer at the background signal, attempting to analyse the origin of the noise rather than just the level.

4.2.4 Power spectral density for $\Omega = 98\,\mathrm{MHz}$

In an effort to remove some of the noise we observed with the modulation frequency of $\Omega = 78\,\mathrm{MHz}$, we did yet another measurement of the noise with a modulation frequency of $\Omega = 98\,\mathrm{MHz}$. The modulation frequency is the frequency that determines how far away from the carrier signal our side-bands are positioned. In the setup (section 3) we implemented a low-pass filter with a cut-off frequency of $140\,\mathrm{MHz}$ immediately after the photodiode, PD#2 in figure 6, in order to cut away any higher-order side-bands. If this low-pass filter does not sufficiently cut off the frequencies, the higher order side-bands will cause unwanted disturbances - noise in our signal. Changing the modulation frequency to $\Omega = 98\,\mathrm{MHz}$ did not seem to neither worsen nor improve our error-signal, and the spectrum in figure 15 was recorded.

The considerations in the previous section also apply to the PSD of the laser modulated with $\Omega = 98\,\mathrm{MHz}$. The general level of the locked laser signal does not appear to have changed much, and certainly not to have fallen, so we must conclude that $\Omega = 98\,\mathrm{MHz}$ does not provide us with a better locking signal than $\Omega = 78\,\mathrm{MHz}$.

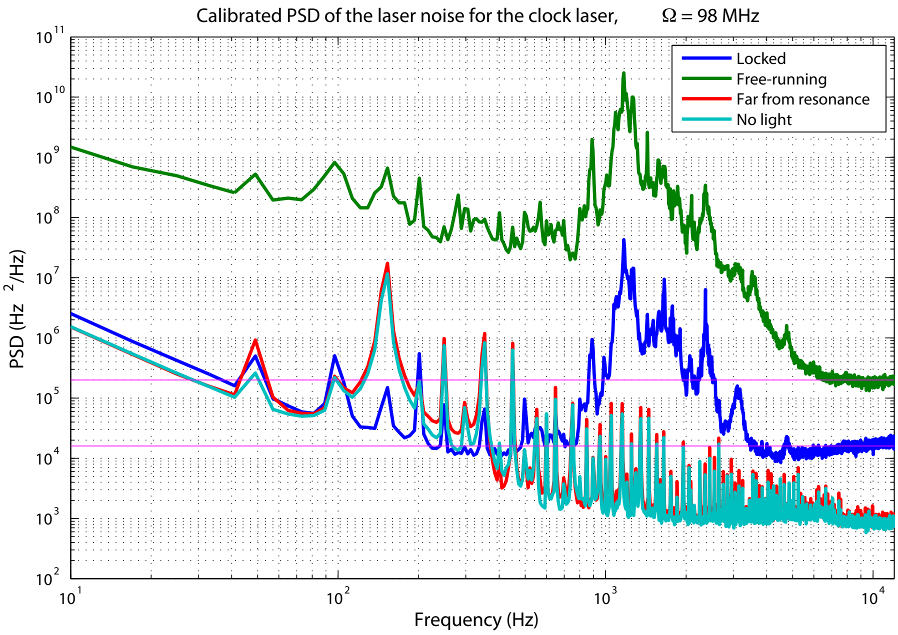

Figure 15: *Power density spectrum of noise for* Ω = 98 *MHz. FFT Bandwidth:* 30.6 *Hz. Horizontal lines indicate white noise floor used for the calculation of Lorentzian linewidth.*

4.2.5 Analysing the spectra

The characteristic Fourier frequencies become interesting when trying to identify the sources of noise.

In Danish power sockets 50 Hz is the frequency of the AC-voltage, and thus a readily identifiable source for 50 Hz noise. Both figure 14 and 15 above show peaks at 50 Hz as well as at harmonic frequencies. The most plausible explanation of these peaks then, is that we have not guarded ourselves well enough in the setup to avoid AC disturbances.

In the case of $\Omega = 78$ MHz, see figure 14, we notice peaks of the locked laser and background noise at 50 Hz, 150 Hz, 250 Hz etc. In the case of $\Omega = 98$ MHz however, we see *all* the harmonics of 50 Hz, at 100 Hz, 150 Hz, 200 Hz, 250 Hz etc. The spectra for $\Omega = 78$ MHz and $\Omega = 98$ MHz respectively were measured on different days allowing for circumstances to change. That we see only the odd harmonics of 50 Hz for $\Omega = 78$ MHz could provide us with a hint to the origin of the source. Having only the odd harmonics corresponds to a square modulation around zero, see figure 16a, and having all harmonics corresponds to a square wave with minimum at zero, see figure 16b. This could indicate that the different distribution of harmonics come from the same source: a square-wave with an oscillating offset. Such a signal could stem from a grounding problem in the setup.

The background noise seems to have fallen slightly in the case of $\Omega = 98$ MHz. Temperature changes or other effects, due to different measuring dates, seem insufficient to explain the factor of 2.5 we see between background and white noise. A plausible cause is effects of the DBM (mixer) as well as the low-pass filter with a cut-off frequency of 140 MHz. A low-pass filter such as ours could readily extinguish notacibly more of the 98 MHz modulation signal than the 78 MHz signal.

Finally, we see a significant bump in all laser spectra at Fourier-frequencies of $1-3$ kHz.

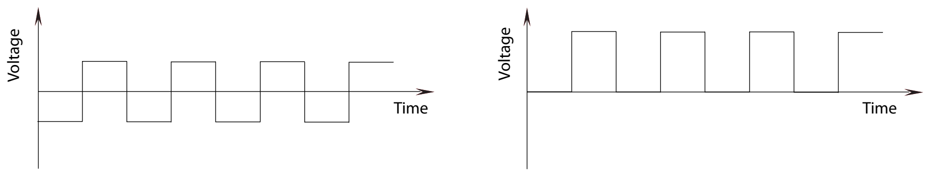

(a) A square-wave oscillating around zero. Odd harmonics.

(b) A square-wave oscillating around an offset with respect to zero. All harmonics.

Figure 16: *Square-waves generated by odd harmonics (a) and all harmonics (b). These might result in the difference of harmonics seen in figure 14 and 15.*

This could stem from acoustic noise. It has to be an effect in the laser light as we do not see the bump in the background spectra. A colleague in the laboratory operating a different laser, but with the same piezo-system implemented in his setup observed a similar bump in his noise-spectra, see figure 17 in appendix A. We conclude that this effect either is a problem with mechanical noise in the piezo-mirror ensemble, or something that affects the whole building (the lab is placed at the fourth floor).

4.2.6 Laser linewidth

In section 2.2.1 we saw that the lineshape of the laser can be calculated from the power spectral density in two different ways, assuming either a Lorentzian or Gaussian lineshape, depending on the ratio $S_\nu(f_c)/f_c$ being much larger or smaller than one respectively.

However, the relation $S_\nu(f_c)/f_c$ does not behave in this way in any of our datasets, and we cannot claim one method to be much better than the other. Rather we will obtain a value from both approximations and compare these two methods in the following.

Results

The results for the Lorentzian approximation is obtained by fitting a constant to the white noise floor, thereby determining S_ν^0. The linewidth is then $\delta\nu = \pi S_\nu^0$.

The results for the Gaussian approximation is obtained by integrating the datapoints numerically:

$$\delta\nu = \sqrt{\Delta f \sum_i S_\nu(f_i)} \qquad \text{for} \qquad 1/T < f_i < f_c, \tag{4.8}$$

where $\Delta f = f_{i+1} - f_i = 8\,\text{Hz}$ is the frequency interval between successive datapoints and $S_\nu(f_i)$ is the power spectral density value of the datapoint. Since the FFT has a bandwidth of 30.6 Hz we use $1/T = 30.6\,\text{Hz}$.

For the laser modulated with 78 MHz, we obtain the linewidth $\delta\nu$:

	Lorentzian	Gaussian*	$S_\nu(f_c)/f_c$
Locked	41 kHz $\pm$ 2 kHz	63 kHz	≈ 3
Free-running	488 kHz $\pm$ 23 kHz	1.34 MHz	≈ 21

For the laser modulated with 98 MHz, we obtain the linewidth $\delta\nu$:

	Lorentzian	Gaussian*	$S_\nu(f_c)/f_c$
Locked	50 kHz ± 3 kHz	61 kHz	≈ 3
Free-running	629 kHz ± 23 kHz	1.49 MHz	≈ 25

* Uncertainties not applicable.

The uncertainties in the linewidth using the Lorentzian lineshape approximation is obtained from the fluctuations of the white noise. The uncertainty is calculated as the standard deviation of S_ν from the fitted white noise floor when we only look at frequencies above the corner frequency.

We have not been able to estimate the uncertainty when the Gaussian lineshape approximation is used. Several complications occur. Firstly, noise is written onto the laser and so the curve of the locked laser in figures 14 and 15 does not give a reliable value of the power spectral density S_ν for low Fourier-frequencies. When integrating the curve numerically, this is suspected to yield an error, resulting in the linewidth estimation becoming too small. Secondly, the determination of the corner frequency f_c is not straightforward. Since we integrate from $1/T$ to f_c, the value of f_c affects the value of the integral.

Furthermore there is an uncertainty associated with each datapoint of S_ν, and this uncertainty is accumulated when we integrate numerically.

The values of $\delta\nu$ obtained by the Gaussian approximation do not differ significantly from the Lorentzian approximation values, and the Gaussian uncertainties are expected to be $\sigma_{\delta\nu_{\text{Gauss}}} \simeq \sigma_{\delta\nu_{\text{Lorentz}}}$. However, since we only have the Lorentzian uncertainties, the values obtained by this approximation seem more reliable.

5 Discussion & Outlook

After stabilizing the laser linewidth by means of the PDH-scheme, we have now obtained a laser linewidth of $\sim 50\,\mathrm{kHz}$, which is an improvement of a factor of 10 compared to the free-running linewidth. We did this using the error-signal obtained from a cavity with linewidth $\sim 9.6\,\mathrm{MHz}$. The further implementation of our setup into the larger-scale experiment will use a cavity of linewidth $8.4\,\mathrm{kHz}$ [6]. The factor of ten improvement to the linewidth we have obtained in the above, greatly increases the stability with which we will be able to lock the laser to this next cavity.

When considering improvements on this system we must remember the objective. The objective here was not to have the most precise stabilization possible, but rather to do a pre-stabilization of the laser prior to a further stabilization using a high-finesse cavity. Factors like the finesse of our cavity then, which intuitively could provide much better stabilization if improved, are not of interest for improvements of this particular setup.

The low finesse of our cavity (~ 124), and thus large linewidth is essential in ensuring that the laser signal does not jump out of resonance with the high-finesse cavity, disabling the lock. Ensuring that the signal does not have any unnecessary noise after this locking, however, is just as essential. In section 4.2.5 we comment on some of the noise of the power spectral densities in figures 14 and 15. All spectra here seem to exhibit noise at harmonics of $50\,\mathrm{Hz}$ as well as in the $1-3\,\mathrm{kHz}$ regime. It seems possible that both of these noise sources could be eliminated thus reducing the noise level further. A colleague in the laboratory is currently working on investigating the piezo control system possibly giving rise to the $1-3\,\mathrm{kHz}$ noise.

Since we have now successfully pre-stabilised the laser the next step will be to couple our PDH-system to the high-finesse PDH-system. The two outputs obtained from these locks cannot simply be plugged into the laser simultaneously. Doing so will result in the two signals 'competing' against each other, and neither of the locks working satisfactory. Rather the signals have to be split up, each controlling their own part of the spectrum.

As our setup is low-finesse and has a large capture-range, it's locking signal will only be used in order to correct for slow variations of frequency. The high-finesse cavity will thus provide an error-signal correcting faster fluctuations. Discrimination of this type can be implemented by using low/high-pass filters and having the two systems correct the laser by different means. Most likely the slow corrections will be controlling a piezo, whereas the fast corrections will control the laser current.

Before implementing the laser as the clock laser in the grand scheme, further investigation of the full PDH-scheme could be interesting. Characterizing the laser noise and linewidth using the PDH-systems each at a time, and finally comparing to the total setup in which they work simultaneously, would be of great interest. This would provide a measure of the effects of implementing this low-finesse system, and, hopefully, give us an indication of the advantages this leads to. We have not conducted these further investigations in this thesis because of the limited time-frame.

6 Conclusion

In the above sections we have described how we have successfully pre-stabilized our laser using the Pound-Drever-Hall technique. We successfully built a PDH-scheme, and generated the error-signal of interest.

Taking advantage of the properties of this signal we have locked the laser frequency, using a feedback signal to the laser current, thus adjusting the frequency. The linewidth of our laser has been reduced by a factor of 10 to a level where the tighter locking to a high-finesse cavity seems much more promising.

While going through the process, we have characterised our Fabry-Perot cavity as well as the residual noise in the locked laser. Using a cavity with a finesse of ~ 124 we have obtained a laser linewidth of $\sim 50\,\mathrm{kHz}$, a first step on the way to reaching a suitable linewidth for experiments with the singlet ${}^1S_0 \leftrightarrow {}^3P_0$ triplet transition of the ^{25}Mg atom.

7 References

[1] B. P. Kibble et al. – *A Realization of the SI Watt by the NPL Moving-coil Balance*
Metrologia, 27 (1990), pp. 173–192.

[2] B. D. Josephson – *Possible new effects in superconductive tunneling*
Phys. Lett., 1 (1962)

[3] *Le Système international d'unités - 8e édition*
Bureau international des poids et mesures, (2006).

[4] T. Rosenband et al. – *Frequency Ratio of Al+ and Hg+ Single-Ion Optical Clocks – Metrology at the 17th Decimal Place*
Science, 319 (2008), pp. 1808–1812.

[5] R. W. P. Drever, J. L. Hall et al. – *Laser Phase and Frequency Stabilization Using an Optical Resonator*
Appl. Phys. B 31 (1983), pp. 97-105.

[6] K. T. Therkildsen – *Investigation of Metastable Magnesium Atoms*
Ph.D Thesis, The Niels Bohr Institute, University of Copenhagen (2009)

[7] E. D. Black – *An Introduction to Pound-Drever-Hall laser frequency stabilization*
Am. J. Phys., Vol.69 (2001), No.1, pp. 79 – 87

[8] F. Riehle – *Frequency Standards – Basics and Applications*
Weinheim (2004)

[9] D. Welford and A. Mooradian – *Observation of linewidth broadening in (GaAl)As diode lasers due to electron number fluctuations*
Appl. Phys. Lett., 40 (1982), pp. 560-562

[10] M. J. O'Mahony and I. D. Henning – *Semiconductor laser linewidth broadening due to $1/f$ carrier noise* Electronics Letters, Vol. 19 No. 23 (1983), pp 1000-1001

[11] G.M. Stéphan et al. – *Laser lineshape and spectral density of frequency noise*
Phys. Rev. A, Vol. 71 (2005), No.4, pp 043809-1 – 9

[12] P. G. Westergaard – *Horloge a réseau optique au Strontium : en quête de la performance ultime*
Ph.D. Thesis, Laboratoire des systèmes de référence temps-espace du LNE (2010)

[13] P. W. Milonni & J. H. Eberly – *Laser Physics*
John Wiley & Sons (2010)

[14] J. R. Taylor – *An introduction to Error Analysis - second edition*
University Science Books (1982)

A Noise spectrum from similar source.

Figure 17 shows the power spectral density (PSD) of a laser similar to ours. The spectra was obtained by our colleague Philip G. Westergaard working in the same laboratory as us. We see a significant bump in the noise around $1 - 3\,\mathrm{kHz}$, just as we have seen in our own spectra (section 4.2) indicating that the noise stems from an inherent noise in the laboratory or from the use of similar equipment (most likely the piezo-systems, which are identical).

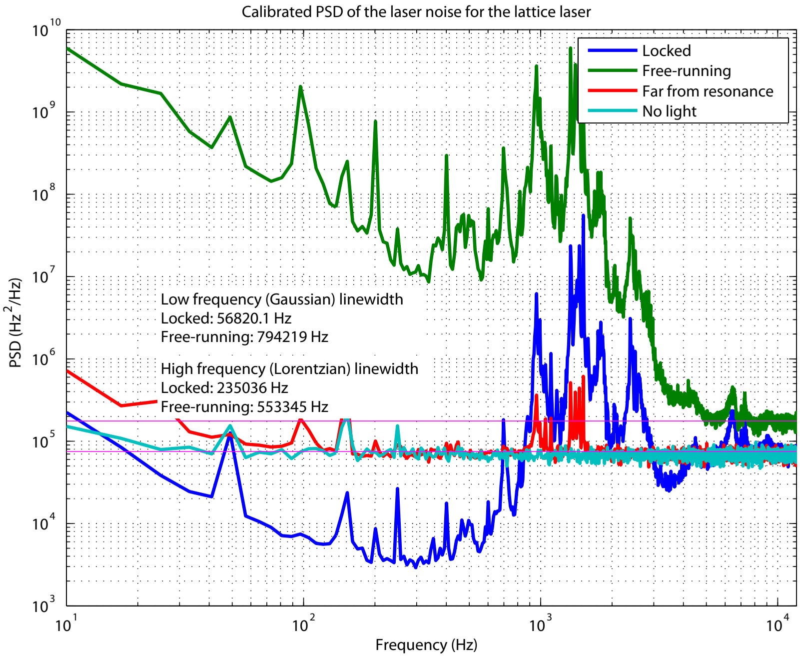

Figure 17: *Power spectral density of different laser in the laboratory (courtesy of Philip G. Westergaard). We here see the same noise around* $1 - 3\,kHz$ *as we did in our own spectra of section 4.2.*